

DRSOM: A Dimension Reduced Second-Order Method

Chuwen Zhang^{*1}, Dongdong Ge¹, Chang He¹, Bo Jiang¹, Yuntian Jiang¹, and Yinyu Ye²

[†]School of Information Management and Engineering, Shanghai University of Finance and Economics

[‡]Department of Management Science and Engineering, Stanford University

January 3, 2023

Abstract

In this paper, we propose a Dimension-Reduced Second-Order Method (DRSOM) for convex and nonconvex (unconstrained) optimization. Under a trust-region-like framework, our method preserves the convergence of the second-order method while using only curvature information in a few directions. Consequently, the computational overhead of our method remains comparable to the first-order such as the gradient descent method. Theoretically, we show that the method has a local quadratic convergence and a global convergence rate of $O(\epsilon^{-3/2})$ to satisfy the first-order and second-order conditions if the subspace satisfies a commonly adopted approximated Hessian assumption. We further show that this assumption can be removed if we perform one *corrector step* (using a Krylov method, for example) periodically at the end stage of the algorithm. The applicability and performance of DRSOM are exhibited by various computational experiments, particularly in machine learning and deep learning. For neural networks, our preliminary implementation seems to gain computational advantages in terms of training accuracy and iteration complexity over state-of-the-art first-order methods such as SGD and ADAM.

1 Introduction

In this paper, we consider the following unconstrained optimization problem

$$\min_{x \in \mathbb{R}^n} f(x), \quad (1)$$

where $f : \mathbb{R}^n \mapsto \mathbb{R}$ is twice differentiable and possibly nonconvex and $f_{\inf} := \inf f(x) > -\infty$. We aim to find a “stationary point” x such that

$$\|\nabla f(x)\| \leq \epsilon \quad (2)$$

and x approximately satisfies the second-order necessary conditions in certain subspace. Historically speaking, various methods have been proposed to solve (1), among which the first-order

^{*}This work is partially supported by the National Natural Science Foundation of China(NSFC) [Grant NSFC-72150001,72225009,72171141,11831002]

methods (FOM) based on the gradient of f are the most popular ones. A first-order method computes a descent direction that iteratively decreases the function value, in which the negative gradient, the momentum [31] can be applied as to construct the iterates. Theoretically, FOMs has the global complexity rate in $O(\epsilon^{-2})$ [26], however, they only converge to a point that satisfies the first-order condition (2).

To escape the first-order stationary point, people may resort to the second-order methods based on the Hessian of f with variants of Newton-type iterations. Traditionally, the global convergence of second-order method can be ensured by frameworks like line search and trust-region methods [28]. While these classical methods are efficient in practice due to local superlinear convergence rate, the global iteration complexity of the standard Newton’s method is generally in the same order as that of the gradient descent method [6]. To clear the mist, Nesterov and Polyak [27] established the first $O(\epsilon^{-3/2})$ iteration complexity for second-order methods using cubic-regularized Newton method (also see Cartis et al. [7, 8]). However, the complexity analysis for the trust-region methods seems to be more challenging. Ye [42] in his early lecture notes showed that the trust-region method with a fixed-radius strategy also has the iteration complexity of $O(\epsilon^{-3/2})$, which matches the iteration bound of the aforementioned cubic regularized Newton method. A more practical *adaptive* trust-region method with $O(\epsilon^{-3/2})$ bound was only unveiled in [15] until very recently.

When the problem dimension gets larger, both explicitly computing the Hessian matrix and solving Newton-type subproblems could be more costly. A practical implementation of the second-order method usually uses a Lanczos method to iteratively find inexact solutions [12, 8, 16], where the “inexactness” can be controlled by the quality of Hessian approximation in some sense [17, 7, 15, 38]. However, even this approach can be impractical for huge-sized problems, e.g., solving sensor-network localization with thousands of sensors and training neural networks involving millions of variables. By contrast, the first-order methods that only require gradient and cheap directions are scalable well to those huge-sized problems. However, their numerical performance heavily relies on *proper* step sizes and other hyperparameters, e.g., using various line search methods [20], and adaptive strategies [22] in stochastic settings. The choice of step size itself requires plentiful experiment and trial procedure. Despite all these difficulties, these methods are prevalent in large scale optimization.

Our approach in this paper is motivated from finding stepsizes for adaptive gradient methods using the Polyak’s momentum [42]. Specifically, we introduce a *Dimension-Reduced Second-Order Method* (DRSOM) to construct and solve a low-dimensional quadratic model to select the stepsizes. The extra overhead of DRSOM is mostly due to constructing and solving such quadratic subproblems.

1.1 Related Work

DRSOM adopts the idea of manipulating the low-dimensional subspace. In optimization, the subspace method is fundamental and widely studied. For example, the gradient method can be

seen as performing a one-dimensional subspace minimization. In trust-region literature, such a minimizer in $\mathcal{L}_k = \text{span}\{g_k\}$ is referred to as the Cauchy point [12]. In comparison, Yuan and Stoer [43] discussed the quadratic approximation over different simple and specific subspaces with an emphasis on their close relationship to the (nonlinear) conjugate gradient method. The authors also provided convergence proofs for the cases based on exact and inexact linear searches. A notable extension of the idea in [43] was made in [34] to the trust-region methods. Briefly speaking, if the subspace is constructed from the previous gradients under the quasi-Newton framework, then one can show that the subspace minimization generates exactly the same iterates of a full-dimensional quasi-Newton algorithm (see [34, Lemma 2.3]). A comprehensive summary on subspace methods can be found in [44, 24].

In contrast with the deterministic setting mentioned above, the *sketching techniques* can also be seen as a *stochastic* subspace method. Early results of sketching appear in solving least-square problems and more generally in numerical linear algebra [36]. The basic idea is to replace the full Hessian with its approximation without destroying the convergence. Using different sketching schemes on the Hessian matrix, Pilanci and Wainwright [30] discussed the convergence rates of the Newton method. This idea later became popular in stochastic second-order optimization [23, 2, 24], and in natural gradient method [39, 40] for training deep neural networks.

As for the momentum-based gradient method, its global convergence rate was only established for convex optimization problems, in terms of the average iterates [19] as well as the last iterate [33]. When the objective function is nonconvex, the sequence generated by the heavy ball method converges to a first-order stationary point [46, 29]. Later, Sun et al. [32] proved that heavy ball method could even escape saddle point. However, the complexity rates are generally not superior to the gradient method under the nonconvex setting¹. A recent work in [1] studied the convergence of heavy ball method under the Polyak–Lojasiewicz condition based on an analysis of the dynamic system.

An earlier line of *modified first-order methods* in the nonconvex case explored the idea of using second-order information in the Nesterov’s accelerated gradient method (AGD), where the momentum direction is also appeared. For example, Carmon et al. [5, 4] used the negative curvature with AGD to achieve a better complexity bound of $O(\epsilon^{-7/4} \log(\epsilon^{-1}))$ for first-order methods. In this vein of research, the improved bound is based on finding the negative curvature with less dimension-dependent complexity². With the help of negative curvature, these methods are able to “escape” from saddle points efficiently and converge to the approximate second-order points in sharp comparison to classical first-order methods.

¹To our best knowledge, we are unaware of better complexity results of Polyak momentum in nonconvex settings

²For example, one can use a randomized Lanczos method which has a complexity bound of $O(\epsilon^{-1/4} \log(\epsilon^{-1}))$

1.2 Our Contribution

In light of the above discussion, this paper extends previous results by demonstrating that one may efficiently enjoy the *charisma* of second-order information while keeping the low per-iteration cost of a first-order method.

- Firstly, we introduce a general dimension-reduced framework DRSOM (Algorithm 1) by solving cheap subproblems without invoking the full Hessian matrix. We further propose some efficient constructions of the low dimensional subproblems. Notably, the DRSOM can be viewed from the subspace perspective [43, 45, 24], however the associated analysis of global and local rates of convergence is missing.
- Secondly, we analyze the convergence of DRSOM based on the discussion in [42]. Under a commonly adopted approximated Hessian assumption (cf. [7, AM.4]), we show that DRSOM has a local quadratic convergence and has an $O(\epsilon^{-3/2})$ complexity to globally converge to a point satisfying the first-order condition (2) and the second-order condition in a certain subspace. We identify that this assumption is only needed at the end stage of the algorithm and can be further removed if we periodically perform a *corrector step*, for example, one step of the Krylov method.
- Finally, we perform comprehensive experiments on convex and nonconvex problems, and finally training neural networks using a mini-batch DRSOM. Our results demonstrate its comparable performance to SOMs (e.g. the Newton trust-region method) in terms of the iteration number and to FOMs (e.g., CG) in terms of the per-iteration cost. For deep learning, our preliminary implementation demonstrates notable advantages in terms of training and testing accuracy over state-of-the-art first-order methods such as SGD and ADAM.

Our paper is organized as follows. In Section 2, we discuss the details of the DRSOM including its important building blocks. Section 3 is regarding the convergence results of DRSOM such as the global convergence rate and local convergence rate. Finally, the comprehensive numerical results of DRSOM are presented in Section 4.

2 The DRSOM

2.1 Notations and Assumptions

We first introduce a few notations and technical lemmas. We denote the standard Euclidean norm by $\|\cdot\|$. If $A \in \mathbb{R}^{n \times n}$, then $\|A\|$ is the induced \mathcal{L}_2 norm and $A \succeq 0$ indicates that A is positive semidefinite. To facilitate discussion, we denote $g_k = g(x_k) = \nabla f(x_k)$, $H_k = H(x_k) = \nabla^2 f(x_k)$, and $d_k = x_k - x_{k-1}$ throughout the paper. We use $\mathcal{N}(\mu, \sigma^2)$ to denote the normal distribution with mean μ , and variance σ^2 .

In the rest of the paper, we assume f is bounded below and is twice differentiable with L -Lipschitz gradient and M -Lipschitz Hessian, which is the standard assumption for second-order

methods.

Assumption 1. f has L -Lipschitz continuous gradient and M -Lipschitz continuous Hessian, i.e., for $\forall x, y \in \mathbb{R}^n$,

$$\|\nabla f(x) - \nabla f(y)\| \leq L\|x - y\| \quad \text{and} \quad \|\nabla^2 f(x) - \nabla^2 f(y)\| \leq M\|x - y\|. \quad (3)$$

The results in the following lemma are also standard and implied by the first- and second-order Lipschitz continuity.

Lemma 1 (Nesterov [26]). *If $f : \mathbb{R}^n \mapsto \mathbb{R}$ satisfies the Assumption 1, then, for all $x, y \in \mathbb{R}^n$,*

$$|f(y) - f(x) - \nabla f(x)^T(y - x)| \leq \frac{L}{2}\|y - x\|^2 \quad (4a)$$

$$\|\nabla f(y) - \nabla f(x) - \nabla^2 f(x)(y - x)\| \leq \frac{M}{2}\|y - x\|^2 \quad (4b)$$

$$\left| f(y) - f(x) - \nabla f(x)^T(y - x) - \frac{1}{2}(y - x)^T \nabla^2 f(x)(y - x) \right| \leq \frac{M}{6}\|y - x\|^3 \quad (4c)$$

We will use the results above repetitively throughout the analysis of the paper.

2.2 Overview of the Algorithm

We now give a brief overview of our method. In each iteration of the Dimension-Reduced Second-Order Method (DRSOM), we update

$$x_{k+1} = x_k - \alpha_k^1 g_k + \alpha_k^2 d_k,$$

and the step size $\alpha_k = (\alpha_k^1, \alpha_k^2)$ is determined by solving the following 2-dimensional quadratic model $m_k(\alpha)$:

$$\begin{aligned} \min_{\alpha \in \mathbb{R}^2} m_k(\alpha) &:= f(x_k) + (c_k)^T \alpha + \frac{1}{2} \alpha^T Q_k \alpha \\ \text{s.t. } \|\alpha\|_{G_k} &:= \sqrt{\alpha^T G_k \alpha} \leq \Delta, \quad \text{with } G_k = \begin{bmatrix} (g_k)^T g_k & -(g_k)^T d_k \\ -(g_k)^T d_k & (d_k)^T d_k \end{bmatrix}, \end{aligned} \quad (5)$$

where

$$Q_k = \begin{bmatrix} (g_k)^T H_k g_k & -(d_k)^T H_k g_k \\ -(d_k)^T H_k g_k & (d_k)^T H_k d_k \end{bmatrix} \in \mathcal{S}^2, \quad c_k = \begin{bmatrix} -\|g_k\|^2 \\ (g_k)^T d_k \end{bmatrix} \in \mathbb{R}^2.$$

The idea of minimizing a low-dimensional quadratic model in the objective was previously studied in Ye [42], Yuan and Stoer [43]. The novel ingredient in this paper is to impose a 2×2 trust-region step to determine the step-sizes, which is necessary for solving nonconvex problems. In particular, the trust-region framework is adopted to ensure the global convergence by controlling the progress made at each step. Similar to the standard trust-region method, after computing a trial step d_{k+1} , we introduce the reduction ratio ρ_k for m_k at iterate x_k ,

$$\rho_k := \frac{f(x_k) - f(x_k + d_{k+1})}{m_k(0) - m_k(\alpha_k)},$$

if ρ_k is too small, especially when $\rho_k < 0$, it means our quadratic model is somehow inaccurate, and it prompts us to decrease the trust region radius; otherwise m_k is good enough, we increase the radius to allow larger search region or keep the radius unchanged.

In the implementation, we also consider the ‘‘Radius-Free’’ DRSOM by dropping the ball constraint in (5) while imposing a quadratic regularization in the objective:

$$\min_{\alpha \in \mathbb{R}^2} m_k(\alpha) + \mu_k \|\alpha\|_{G_k}^2. \quad (6)$$

The regularization parameter μ_k can be tuned to achieve the effect of expanding or contracting the trust region by increasing or decreasing the value of μ_k .

In the following, we present a conceptual DRSOM in Algorithm 1 by incorporating the two alternatives (5) and (6) to compute the step size α , where the adaptive strategy to update the radius of the trust-region constraint or the coefficient of the quadratic regularization is adopted.

Algorithm 1: A conceptual DRSOM algorithm

Data: Given $k_{\max}, \beta_1 < 1 < \beta_2, \zeta_1 < \zeta_2 \leq 1; \bar{\Delta} > 0, \Delta_0 \in (0, \bar{\Delta})$, and $\eta \in [0, \zeta_1)$;

```

1 for  $k = 1, \dots, k_{\max}$  do
2   | Solve (5) or (6) for  $\alpha_k$ ;
3   | Compute  $d_{k+1} = -\alpha_k^1 g_k + \alpha_k^2 d_k$  and  $\rho_k := \frac{f(x_k) - f(x_k + p_k)}{m_k(0) - m_k(p_k)}$ ;
4   | if  $\rho_k > \eta$  then
5   |   | Accept the step and update  $x_{k+1} = x_k + d_{k+1}$ 
6   |   | else
7   |   |   | Adjust  $\Delta_k$  in (5) or  $\mu_k$  in (6)
8   |   |   | end
9 end

```

In the following, we provide two alternatives to efficiently construct the low-dimensional quadratic model, where the full Hessian matrix is not needed.

Constructing 2-D Quadratic Model Using HVPs To efficiently compute the 2×2 matrix Q_k in (5), we make use of the decomposition

$$Q_k = [-g_k, d_k]^T [-H_k \cdot g_k, H_k \cdot d_k].$$

Thus, it remains to compute the two Hessian-vector products (HVP) (see [28]): $H_k g_k$ and $H_k d_k$. We adopt the following two strategies to compute those products without request for the full Hessian H_k :

1. Finite difference: $H_k \cdot v \approx \frac{1}{\epsilon} [g(x_k + \epsilon \cdot v) - g_k]$; $v \in \{g_k, d_k\}$.
2. Automatic differentiation (AD): $H_k g_k = \nabla(\frac{1}{2} g_k^T g_k)$, $H_k d_k = \nabla(d_k^T g_k)$.

Constructing 2-D Quadratic Model Using Interpolation Besides HVPs, DRSOM can further benefit from zero-order minimization techniques [14, 11] and use interpolation to construct the quadratic model. In particular, given g_k, d_k at iteration k , we write the quadratic model:

$$\begin{aligned} m_k(-\alpha_k^1 g_k + \alpha_k^2 d_k) &= c_k^T \alpha_k + Q_k \bullet \frac{1}{2} \alpha_k \alpha_k^T \\ &= c_k^T \alpha_k + q_k^T p_2(\alpha_k), \end{aligned} \quad (7)$$

where $c_k = [-\|g_k\|^2, g_k^T d_k]$ is known, $q_k := [Q_{11}, Q_{12}, Q_{22}]^T$ is the vectorized upper-triangular part of Q_k , and

$$p_2(\alpha_k) := \left[\frac{(\alpha_k^1)^2}{2}, \alpha_k^1 \alpha_k^2, \frac{(\alpha_k^2)^2}{2} \right]^T \quad (8)$$

is the monomial basis of $\alpha_k \in \mathbb{R}^2$ with order 2. We see that if using quadratic interpolation (with exact gradient), the monomial bases are constructed with respect to the *stepsizes* to solve q_k with 3 unknown entries, which is independent of the problem dimension. To determine the solution, the task left here is to generate an *interpolation set* containing $\ell \geq 3$ different stepsizes, namely $\beta_1, \dots, \beta_\ell$. After that, we will have a linear system forming from ℓ extra function evaluations by setting α_k to $\beta_1, \dots, \beta_\ell$ respectively. By Taylor expansion and (7), it follows that:

$$f(x_k - \alpha_k^1 g_k + \alpha_k^2 d_k) = f(x_k) + c_k^T \alpha_k + q_k^T p_2(\alpha_k) + O(\|-\alpha_k^1 g_k + \alpha_k^2 d_k\|^3)$$

Therefore, we solve the following equations with the monomial matrix on the left-hand side:

$$\begin{bmatrix} p_2(\beta_1)^T \\ \dots \\ p_2(\beta_\ell)^T \end{bmatrix} \cdot q_k = \begin{bmatrix} f(x_k - \beta_1^1 g_k + \beta_1^2 d_k) - f(x_k) - c_k^T \beta_1 \\ \dots \\ f(x_k - \beta_\ell^1 g_k + \beta_\ell^2 d_k) - f(x_k) - c_k^T \beta_\ell \end{bmatrix}. \quad (9)$$

For computation, the monomial matrix has to be nonsingular. We adopt a simple strategy and randomly pick $\beta_1, \dots, \beta_\ell$ over the unit sphere. In theory, if the iterate moves in the convex hull of sample points, then the error between the function value and the estimation can be uniformly bounded; besides, one can choose more samples so as to alleviate the noise factors [13]. In practice, we find that the interpolation method is highly efficient in practice.

In our experience, the interpolation method is preferred over the methods based on finite difference and HVP in most cases in terms of computational speed.

2.3 Preliminaries of DRSOM

In this subsection, we present some preliminary analysis of DRSOM. We introduce the following Lemma regarding the global solution of (5) which is widely known.

Lemma 2. *The vector α^* is the global solution to trust-region subproblem (5) if it is feasible and there exists a Lagrange multiplier $\lambda^* \geq 0$ such that (α^*, λ^*) is the solution to the following equations:*

$$(Q_k + \lambda G_k) \alpha + c_k = 0, Q_k + \lambda G_k \succeq 0, \lambda(\Delta - \|\alpha\|_{G_k}) = 0. \quad (10)$$

From the construction of Q_k and G_k , we have that

$$Q_k + \lambda G_k = \begin{bmatrix} -g_k^T \\ d_k^T \end{bmatrix} (H_k + \lambda I) \begin{bmatrix} -g_k & d_k \end{bmatrix}. \quad (11)$$

Therefore, even if Q_k is indefinite, there always exists a sufficiently large λ such that condition (10) holds. Ye [41] showed that an ϵ -global primal-dual optimizer (α^*, λ^*) satisfying (10) can be found in $O(\log \log(1/\epsilon))$ time. One may also find the optimal solutions by other standard methods in Conn et al. [12]. Due to the fact that we only use two directions, the associated subproblems are easy to solve.

We also introduce the normalized problem to facilitate analysis:

$$\begin{aligned} \min_{\alpha \in \mathbb{R}^2} \quad & f(x_k) + \alpha^T V_k^T g_k + \frac{1}{2} \alpha^T V_k^T H_k V_k \alpha \\ \text{s.t.} \quad & \|\alpha\| \leq \Delta_k, \end{aligned} \quad (12)$$

where V_k is the orthonormal bases for $\mathcal{L}_k := \text{span}\{g_k, d_k\}$. It is worth mentioning that most of our analysis still goes through for general subspace \mathcal{L}_k , although the form of \mathcal{L}_k is specified in DR-SOM. It is easy to see (12) and (5) are equivalent under a linear transformation. With a slightly abuse of notation, we do not differentiate α_k and the dual variable λ_k to those in (5). In the next lemma, we note that although problem (5) is a 2-dimensional trust region model, its solution can be transformed into a solution of the ‘‘full-scale’’ trust-region problem, as shown below.

Lemma 3. *Let α_k and λ_k be the solution and the associated Lagrangian multiplier with the trust region constraint to the normalized problem (12). Construct $d_{k+1} = V_k \alpha_k$, then d_{k+1} is a solution to the full-scale problem*

$$\min_{d \in \mathbb{R}^n} \quad \tilde{m}_k(d) := f(x_k) + g_k^T d + \frac{1}{2} d^T \tilde{H}_k d, \quad \text{s.t.} \quad \|d\| \leq \Delta, \quad (13)$$

such that

$$(\tilde{H}_k + \lambda_k I) d_{k+1} + g_k = 0, \quad \tilde{H}_k + \lambda_k I \succeq 0, \quad \lambda_k (\|d_{k+1}\| - \Delta_k) = 0, \quad (14)$$

where $\tilde{H}_k = V_k V_k^T H_k V_k V_k^T$.

Proof. According to (10), we have that

$$(V_k^T H_k V_k + I) \alpha_k + V_k^T g_k = 0, \quad V_k^T H_k V_k + \lambda_k I \succeq 0, \quad \lambda_k (\Delta - \|\alpha_k\|) = 0. \quad (15)$$

Multiplying V_k to the left of both sides of the first equation in (15) yields that

$$V_k V_k^T H_k V_k V_k^T V_k \alpha_k + \lambda_k V_k \alpha_k = V_k V_k^T H_k V_k \alpha_k + \lambda_k V_k \alpha_k = -V_k V_k^T g_k = -g_k,$$

where the first equality is due to $V_k^T V_k = I$ and the last equality follows from $V_k V_k^T$ is the projection matrix of \mathcal{L}_k and $g_k \in \mathcal{L}_k$. As a result, we have that:

$$(V_k V_k^T H_k V_k V_k^T + \lambda_k I) d_{k+1} + g_k = 0$$

proving the first equation in (14). Due to the second equation in (15), we have that

$$\alpha^T V_k^T H_k V_k \alpha + \lambda_k \alpha^T \alpha \geq 0, \forall \alpha \in \mathbb{R}^2.$$

By letting $d = V_k \alpha$, it is equivalent to

$$d^T H_k d + \lambda_k d^T d \geq 0, \forall d \in \mathcal{L}_k$$

due to V_k is the orthonormal bases for \mathcal{L}_k and $d^T d = \alpha^T V_k^T V_k \alpha = \alpha^T \alpha$. The inequality above is further equivalent to

$$\tilde{d}^T (V_k V_k^T H_k V_k V_k^T + \lambda_k I) \tilde{d} \geq 0, \forall \tilde{d} \in \mathbb{R}^n$$

as $V_k V_k^T$ is the projection matrix of \mathcal{L}_k , and this proves $\tilde{H}_k + \lambda I \succeq 0$ in (14). Finally, since $d_{k+1}^T d_{k+1} = \alpha_k^T V_k^T V_k \alpha_k = \alpha_k^T \alpha_k$, the last equation in (14) follows from the last equation in (15). Therefore, d_{k+1} is a solution to the problem (13). \square

The merit of problem (13) is that we do not require the constraint $d \in \mathcal{L}_k$ and shift the subspace restriction to the matrix \tilde{H}_k , which can be viewed as the projection of the original Hessian H_k in the subspace \mathcal{L}_k . Therefore, \tilde{H}_k plays the same role as the approximated Hessian matrix in the inexact Newton method, and DR-SOM may similarly be regarded as a cheap quasi-Newton method. In the computations, we actually solve the 2-dimensional quadratic problem (5) for the sake of convenience. However, the facts established for its full-scale counterpart (13) will be frequently used in the convergence analysis of DR-SOM.

3 Convergence Results

In this section, we provide a suite of convergence results of DR-SOM. Our analysis includes the equivalence between DR-SOM and conjugate gradient (CG) method for strongly convex quadratic programming, the global convergence rate and the local convergence rate of DR-SOM for nonconvex setting. Although the subproblem of DR-SOM is constrained to a two dimensional (gradient g_k and momentum d_k) subspace, the global and local convergence rate analysis could be extended to the general subspace that is not restricted to be spanned by g_k and d_k . Our analysis shows that if the subspace produces a sufficiently good approximated Hessian, DR-SOM can achieve extraordinary convergence rate both globally and locally.

3.1 Finite Convergence for Strongly Convex Quadratic Programming

We first show DR-SOM has finite convergence for strongly convex quadratic programming.

$$\min f(x) = \frac{1}{2} x^T A x + a^T x, \quad (16)$$

where $A \succ 0$. In this case, we drop the trust-region constraint for DR-SOM, i.e., Δ_k is sufficiently large, $\lambda_k = 0$ for all k . We have the following theorem.

Theorem 1. *If we apply DRSOM to (16) with no radius restriction, i.e., Δ is sufficiently large, then the DRSOM generates the same iterates of conjugate gradient method, if they start at the same point x_0 .*

Proof. To show its equivalence to the conjugate gradient method, we only have to prove the iterate x_k by DRSOM minimizes $f(x)$ in the subspace such that:

$$x_k \in \mathcal{L}_k = x_0 + \text{span}\{d_1, \dots, d_k\}.$$

Since there is no radius, the solution that minimizes m_k strictly corresponds to the optimizer of $f(x)$ in the subspace $x_k + \text{span}\{g_k, d_k\}$. In other words, the iterate of DRSOM can also be retrieved by simply choosing the stepsizes such that $x_{k+1} = \arg \min f(x)$ and $x_{k+1} = x_k - \alpha_k^1 g_k + \alpha_k^2 d_k$. From such a perspective, we show that the x_k is equivalent to \tilde{x}_k by the conjugate gradient method.

Note \tilde{x}_k minimizes $f(x)$ over the subspace below:

$$x_0 + \text{span}\{\tilde{d}_1, \dots, \tilde{d}_k\},$$

where $\tilde{d}_1, \dots, \tilde{d}_k$ are conjugate directions for CG. By construction, we see $x_1 = x_0 + \alpha_0^1 g_0$ and $d_1 = \alpha_0^1 g_0$, so that $x_1 = \tilde{x}_1$. Assume it holds for k , we know for CG:

$$\tilde{g}_k \in \text{span}\{\tilde{d}_k, \tilde{d}_{k+1}\},$$

and since $g_k = \tilde{g}_k$, $d_k = \tilde{d}_k$, we have

$$\text{span}\{\tilde{d}_k, \tilde{d}_{k+1}\} = \text{span}\{d_k, g_k\}, \quad (17)$$

Now we know from the next minimizer $x_{k+1} \in x_k + \text{span}\{d_k, g_k\}$:

$$x_{k+1} \in \tilde{x}_k + \text{span}\{\tilde{d}_k, \tilde{d}_{k+1}\},$$

and since \tilde{x}_{k+1} minimizes f over both $x_0 + \text{span}\{d_1, \dots, d_k, \tilde{d}_{k+1}\}$ and $x_k + \text{span}\{\tilde{d}_{k+1}\}$, we have that $x_{k+1} = \tilde{x}_{k+1}$ as the desired result. \square

The equivalence of quadratic minimization over \mathcal{L}_k and conjugate gradient method was also established in Yuan and Stoer [43]. We provide the proof of Theorem 1 for the completeness of the paper.

3.2 Global Convergence Rate

To analyze the convergence rate of DRSOM, we need to make the following assumption regarding the approximated Hessian \tilde{H}_k , which is commonly used in the literature; see [17, 8, 15, 38].

Assumption 2. *The approximated Hessian matrix \tilde{H}_k along subspace \mathcal{L}_k satisfies:*

$$\|(H_k - \tilde{H}_k)d_{k+1}\| \leq C\|d_{k+1}\|^2 \quad (18)$$

Although we adopt the adaptive strategy to choose the radius in the implementation, our analysis is conducted under the fixed-radius strategy such that a step is always accepted for simplicity. In terms of the global convergence rate, we show that DR-SOM has an $O(\epsilon^{-3/2})$ complexity to converge to the first-order stationary point and second-order point approximately in the subspace. Let us assume that [Assumption 2](#) holds for the following analysis.

To prove our main theorem, we need to establish the following lemma as preparation.

Lemma 4 (Model reduction). *At iteration k , let d_{k+1} and λ_k be the solution and Lagrangian multiplier constructed in [Lemma 3](#). If $\lambda_k > 0$, we have the following amount of decrease on \tilde{m}_k :*

$$\tilde{m}_k(d_{k+1}) - \tilde{m}_k(0) = -\frac{1}{2}\lambda_k\Delta_k^2. \quad (19)$$

Proof. In view of [Lemma 3](#), the optimal condition (14) holds. Then, we have $\|d_{k+1}\| = \Delta_k$ due to $\lambda_k > 0$ and that:

$$\begin{aligned} \tilde{m}_k(d_{k+1}) - \tilde{m}_k(0) &= g_k^T d_{k+1} + \frac{1}{2}d_{k+1}^T \tilde{H}_k d_{k+1} \\ &= -\frac{1}{2}d_{k+1}^T (\tilde{H}_k + \lambda_k I) d_{k+1} + \frac{1}{2}d_{k+1}^T \tilde{H}_k d_{k+1} \\ &= -\frac{1}{2}\lambda_k\Delta_k^2, \end{aligned} \quad (20)$$

which completes the proof. \square

Taking $\Delta_k = \Delta = \frac{2\sqrt{\epsilon}}{M}$ and combining with the reduction of the quadratic model, we conclude that DR-SOM generates sufficient decrease at every iteration k as long as $\lambda_k \geq \sqrt{\epsilon}$. The following analysis based on a *fixed* trust-region radius is motivated from Luenberger and Ye [25].

Lemma 5 (Sufficient decrease). *At iteration k , take $\Delta_k = \Delta = \frac{2\sqrt{\epsilon}}{M}$, and let d_{k+1} and λ_k be the solution and Lagrangian multiplier obtained in [Lemma 3](#). If $\lambda_k \geq \sqrt{\epsilon}$, we have the following amount of function value decrease,*

$$f(x_{k+1}) \leq f(x_k) - \frac{2}{3M^2}\epsilon^{3/2}. \quad (21)$$

Proof. Since $d_{k+1} \in \mathcal{L}_k$ and $V_k V_k^T$ is the projection matrix of \mathcal{L}_k , it holds that

$$d_{k+1}^T \tilde{H}_k d_{k+1} = d_{k+1}^T V_k V_k^T H_k V_k V_k^T d_{k+1} = d_{k+1}^T H_k d_{k+1}.$$

Moreover, with second-order Lipschitz continuity and Taylor expansion, we immediately have:

$$\begin{aligned} f(x_{k+1}) &\leq f(x_k) + (g_k)^T d_{k+1} + \frac{1}{2}(d_{k+1})^T H_k(d_{k+1}) + \frac{M}{6}\|d_{k+1}\|^3 \\ &= f(x_k) + (g_k)^T d_{k+1} + \frac{1}{2}(d_{k+1})^T \tilde{H}_k(d_{k+1}) + \frac{M}{6}\|d_{k+1}\|^3 \\ &= f(x_k) - \frac{1}{2}\lambda_k\Delta^2 + \frac{1}{6}M\Delta^3 \\ &= f(x_k) - \frac{2\lambda_k\epsilon}{M^2} + \frac{4\epsilon^{3/2}}{3M^2} \end{aligned} \quad (22)$$

where the second last equality is due to [Lemma 4](#) and $\|d_{k+1}\| = \Delta_k = \Delta$ from the optimality condition (14) with $\lambda_k > 0$. Noting that $\lambda_k \geq \sqrt{\epsilon}$, inequality (22) implies that

$$f(x_{k+1}) \leq f(x_k) - \frac{2}{3M^2}\epsilon^{3/2}.$$

□

The following result states that when $\lambda_k \leq \sqrt{\epsilon}$ and the Hessian regularity condition holds, we can terminate the process at the next iterate x_{k+1} that approximated satisfies the first-order condition and the second-order condition in the subspace.

Lemma 6. *At iteration k , if the Lagrangian multiplier λ_k associated with the trust region constraint in (5) satisfies $\lambda_k \leq \sqrt{\epsilon}$ and Hessian regularity condition (18) holds, then the iterate x_{k+1} approximately satisfies the first-order condition, and the second-order condition in the subspace \mathcal{L}_k .*

Proof. Suppose d_{k+1} is the solution obtained in [Lemma 3](#). By second-order Lipschitz continuity and the first equation in the optimality condition (14), we have that:

$$\begin{aligned} \|g_{k+1}\| &\leq \|g_{k+1} - g_k - H_k d_{k+1}\| + \|(H_k - \tilde{H}_k)d_{k+1}\| + \|(g_k + \tilde{H}_k d_{k+1})\| \\ &\leq \left\| \int_0^1 [\nabla^2 f(x_k + \tau d_{k+1}) - H_k] d_{k+1} d\tau \right\| + \|(H_k - \tilde{H}_k)d_{k+1}\| + \lambda_k \|d_{k+1}\| \\ &\leq \frac{1}{2}M\|d_{k+1}\|^2 + \lambda_k \|d_{k+1}\| + \|(H_k - \tilde{H}_k)d_{k+1}\| \end{aligned} \quad (23)$$

In view of [Assumption 2](#), $\lambda_k \leq \sqrt{\epsilon}$ and $\|d_{k+1}\| \leq \Delta = \frac{2\sqrt{\epsilon}}{M}$, we immediately have

$$\begin{aligned} \|g_{k+1}\| &\leq \left(\frac{1}{2}M + C\right) \|d_{k+1}\|^2 + \lambda_k \|d_{k+1}\| \\ &\leq \left(\frac{1}{2}M + C\right) \frac{4\epsilon}{M^2} + \frac{2\epsilon}{M} \\ &\leq \left(\frac{4}{M} + \frac{4C}{M^2}\right) \epsilon. \end{aligned} \quad (24)$$

As for the second-order condition, the second condition in (14) and $\lambda_k \leq \sqrt{\epsilon}$ imply that

$$\begin{aligned} -\sqrt{\epsilon}I &\preceq -\lambda_k I \preceq \tilde{H}_k = V_k V_k^T H_{k+1} V_k V_k^T + \tilde{H}_k - V_k V_k^T H_{k+1} V_k V_k^T \\ &= V_k V_k^T H_{k+1} V_k V_k^T + V_k V_k^T (H_k - H_{k+1}) V_k V_k^T \\ &\preceq V_k V_k^T H_{k+1} V_k V_k^T + \|V_k V_k^T (H_k - H_{k+1}) V_k V_k^T\| I \\ &\preceq V_k V_k^T H_{k+1} V_k V_k^T + \|V_k V_k^T\| \|H_{k+1} - H_k\| \|V_k V_k^T\| I \\ &= V_k V_k^T H_{k+1} V_k V_k^T + \|H_{k+1} - H_k\| I \\ &\preceq V_k V_k^T H_{k+1} V_k V_k^T + M \|d_{k+1}\| I \\ &\preceq V_k V_k^T H_{k+1} V_k V_k^T + 2\sqrt{\epsilon}I, \end{aligned} \quad (25)$$

where the second last matrix inequality is due to the Lipschitz continuity of the Hessian and the last matrix inequality follows from $\|d_{k+1}\| \leq \Delta = \frac{2\sqrt{\epsilon}}{M}$. Hence, it holds that

$$V_k V_k^T H_{k+1} V_k V_k^T \succeq -3\sqrt{\epsilon}I,$$

which indicates that H_{k+1} is approximately positive semi-definite in the subspace \mathcal{L}_k . \square

Theorem 2. *Under the fixed-radius strategy by setting $\Delta_k = \frac{2\sqrt{\epsilon}}{M}$, the DRSOM runs at most $O\left(\frac{3}{2}M^2(f(x_0) - f_{\inf})\epsilon^{-3/2}\right)$ iterations to reach an iterate x_{k+1} that satisfies the first-order condition (2), and the approximated second-order condition in the subspace \mathcal{L}_k : $V_k V_k^T H_{k+1} V_k V_k^T \succeq -3\sqrt{\epsilon}I$, where V_k is the orthonormal bases for \mathcal{L}_k .*

Proof. According to Lemma 6, when $\lambda_k \leq \sqrt{\epsilon}$, we already obtain an iterate that approximately satisfies the first-order condition, and the second-order condition in certain subspace. On the other hand, when $\lambda_k > \sqrt{\epsilon}$, Lemma 5 indicates that the objective function has a amount of decrease $\frac{2}{3M^2}\epsilon^{3/2}$ at every iteration k . Note that the total amount of decrease cannot exceed $f(x_0) - f_{\inf}$. Therefore, the number of iterations with $\lambda_k > \sqrt{\epsilon}$ is upper bounded by

$$O\left(\frac{3}{2}M^2(f(x_0) - f_{\inf})\epsilon^{-3/2}\right),$$

which thus is also the iteration bound of our algorithm. \square

3.3 Local Convergence Rate

Regarding the local rate of convergence, we can prove that DRSOM have a local quadratic convergence rate. To this end, we first present some technical lemmas.

Lemma 7. *Let V_k be the orthonormal bases for \mathcal{L}_k , suppose α_k is the solution to the normalized problem (12). Let $d_{k+1} = V_k \alpha_k$, then the following inequality holds:*

$$\|d_{k+1}^{SN} - d_{k+1}\| \leq \frac{1}{\mu} \lambda_k \|d_{k+1}\|, \quad (26)$$

where λ_k is the Lagrangian multiplier associated with the trust region constraint in (12), and $d_{k+1}^{SN} = V_k \alpha_k^{SN}$ is the subspace Newton step with α_k^{SN} defined by:

$$\alpha_k^{SN} = \arg \min_{\alpha \in \mathbb{R}^2} f(x_k) + \alpha^T V_k^T g_k + \frac{1}{2} \alpha^T V_k^T H_k V_k \alpha. \quad (27)$$

Proof. Since α_k is a solution to the normalized problem (12), the optimality condition gives that

$$(V_k^T H_k V_k + \lambda_k I) \alpha_k = -g_k^T V_k.$$

As α_k^{SN} is a solution to problem (26), due to optimality condition it holds that

$$V_k^T H_k V_k \alpha_k^{SN} = -g_k^T V_k.$$

Combining the above two equations yields that

$$V_k^T H_k V_k (\alpha_k - \alpha_k^{SN}) = -\lambda_k \alpha_k. \quad (28)$$

Moreover, note that

$$\text{for any } \alpha \neq 0, \text{ we have } V_k \alpha \neq 0 \text{ and } \|V_k \alpha\| = \|\alpha\|, \quad (29)$$

which combined with $H_k \succeq \mu I$ implies that

$$\alpha^T V_k^T H_k V_k \alpha \geq \mu \|V_k \alpha\|^2 = \mu \|\alpha\|^2.$$

Therefore $V_k^T H_k V_k \succeq \mu I_2$ holds (also implies that $V_k^T H_k V_k$ is nonsingular), it follows that

$$\|\alpha_k^{SN} - \alpha_k\| \leq \|(V_k^T H_k V_k)^{-1}\| \|V_k^T H_k V_k (\alpha_k^{SN} - \alpha_k)\| \leq \frac{1}{\mu} \lambda_k \|\alpha_k\|, \quad (30)$$

where the second inequality is due to (28). Therefore, by combining the construction of d_{k+1}^{SN} and d_{k+1} with (29) we conclude that

$$\|d_{k+1}^{SN} - d_{k+1}\| = \|\alpha_k^{SN} - \alpha_k\| \leq \frac{1}{\mu} \lambda_k \|\alpha_k\| = \frac{1}{\mu} \lambda_k \|d_{k+1}\|. \quad (31)$$

□

We now ready to provide the following key result to analyze the local convergence rate of our algorithm, where we assume it converges to a strict local optimum x^* such that $H(x^*) \succeq \mu I$ for some $\mu > 0$.

Lemma 8. *Suppose the iterate of DRSON x_k converges to x^* which satisfies $H(x^*) \succeq \mu I$, when x_k is sufficiently close to x^* , then we have:*

$$\|x_{k+1} - x^*\| \leq \frac{M}{\mu} \|x_k - x^*\|^2 + \frac{1}{\mu} \|(H_k - \tilde{H}_k) d_{k+1}\| + \left(\frac{2L}{\mu^2} + \frac{1}{\mu} \right) \lambda_k \|d_{k+1}\|. \quad (32)$$

Proof. We first write

$$\begin{aligned} \|x_{k+1} - x^*\| &= \|x_k + d_{k+1} - x^*\| \\ &\leq \|x_k + d_{k+1}^N - x^*\| + \|d_{k+1}^{SN} - d_{k+1}^N\| + \|d_{k+1} - d_{k+1}^{SN}\|, \end{aligned} \quad (33)$$

where $d_{k+1}^N = -H_k^{-1} g_k$ is the standard Newton step and $d_{k+1}^{SN} = V_k \alpha_k^{SN}$ is the subspace Newton step with α_k^{SN} defined by (27). The first term in (33) is upper bounded by $\frac{M}{\mu} \|x_k - x^*\|^2$ due to the standard analysis in Newton's method. To bound the second term, we note that $\alpha_k^{SN} = (V_k^T H_k V_k)^{-1} V_k^T g_k$ with $V_k^T V_k = I$ as it is a solution to problem (27), which implies that

$$\begin{aligned} \tilde{H}_k d_{k+1}^{SN} &= \tilde{H}_k V_k (V_k^T H_k V_k)^{-1} V_k^T g_k \\ &= V_k V_k^T H_k V_k V_k^T V_k (V_k^T H_k V_k)^{-1} V_k^T g_k \\ &= V_k V_k^T g_k = g_k, \end{aligned}$$

where the last equality is due to $V_k V_k^T$ is the projection matrix of the subspace \mathcal{L}_k and $g_k \in \mathcal{L}_k$. Then, the second term can be further bounded above as follows

$$\begin{aligned}
\|d_{k+1}^{SN} - d_{k+1}^N\| &= \|d_{k+1}^{SN} + H_k^{-1}g_k\| \\
&= \|d_{k+1}^{SN} - H_k^{-1}\tilde{H}_k d_{k+1}^{SN}\| \\
&= \|H_k^{-1}(H_k - \tilde{H}_k)d_{k+1}^{SN}\| \\
&\leq \|H_k^{-1}\| \|(H_k - \tilde{H}_k)d_{k+1}^{SN}\| \\
&\leq \frac{1}{\mu} \|(H_k - \tilde{H}_k)d_{k+1}^{SN}\| \\
&\leq \frac{1}{\mu} \left(\|(H_k - \tilde{H}_k)d_{k+1}\| + \|(H_k - \tilde{H}_k)(d_{k+1}^{SN} - d_{k+1})\| \right) \\
&\leq \frac{1}{\mu} \|(H_k - \tilde{H}_k)d_{k+1}\| + \frac{1}{\mu} \|H_k - \tilde{H}_k\| \|(d_{k+1}^{SN} - d_{k+1})\|, \tag{34}
\end{aligned}$$

Combining the above inequalities, we have that

$$\begin{aligned}
&\|x_{k+1} - x^*\| \\
&\leq \frac{M}{\mu} \|x_k - x^*\|^2 + \frac{1}{\mu} \|(H_k - \tilde{H}_k)d_{k+1}\| + \left(\frac{1}{\mu} \|H_k - \tilde{H}_k\| + 1 \right) \|d_{k+1} - d_{k+1}^{SN}\| \tag{35} \\
&\leq \frac{M}{\mu} \|x_k - x^*\|^2 + \frac{1}{\mu} \|(H_k - \tilde{H}_k)d_{k+1}\| + \left(\frac{2L}{\mu^2} + \frac{1}{\mu} \right) \lambda_k \|d_{k+1}\|,
\end{aligned}$$

where the last inequality follows from [Lemma 7](#) and $\max\{\|H_k\|, \|\tilde{H}_k\|\} \leq L$ due to the Lipschitz continuity of the gradient. \square

Theorem 3. *Suppose x^* is a second-order stationary point such that $H(x^*) \succeq \mu I$ for some $\mu > 0$. Then if x_k is sufficiently close to x^* , DR-SOM converges to x^* quadratically, namely: $\|x_{k+1} - x^*\| \leq O(\|x_k - x^*\|^2)$.*

Proof. It suffices to further upper bound (32). We only consider the scenario that $\lambda_k \leq \sqrt{\epsilon}$, as otherwise, the objective function has an amount of decrease $\frac{2}{3M^2}\epsilon^{3/2}$ at every iteration k by [Lemma 5](#) and this will occur in a very limited time when x_k is sufficiently close to x^* .

Since (18) holds, one has that

$$\frac{1}{\mu} \|(H_k - \tilde{H}_k)d_{k+1}\| \leq \frac{C}{\mu} \|d_{k+1}\|^2.$$

Moreover, as we adopt the fixed radius strategy, $\lambda_k = 0$ whenever $\|d_{k+1}\| < \Delta$. In the case of $0 < \lambda_k \leq \sqrt{\epsilon}$, we have $\lambda_k \leq \sqrt{\epsilon} = \frac{M}{2}\Delta = \frac{M}{2}\|d_{k+1}\|$. Therefore, in both cases, we have $\lambda_k \|d_{k+1}\| \leq \frac{M}{2} \|d_{k+1}\|^2$. Consequently, (32) can be bounded above by

$$\|x_{k+1} - x^*\| \leq \frac{M}{\mu} \|x_k - x^*\|^2 + \frac{C}{\mu} \|d_{k+1}\|^2 + \left(\frac{2L}{\mu^2} + \frac{1}{\mu} \right) \frac{M}{2} \|d_{k+1}\|^2.$$

Note that

$$\begin{aligned}
\|d_{k+1}\| &\leq \|x_k - x^* + d_{k+1}\| + \|x_k - x^*\| \\
&= \|x_{k+1} - x^*\| + \|x_k - x^*\| \\
&\leq \frac{M}{\mu} \|x_k - x^*\|^2 + \frac{C}{\mu} \|d_{k+1}\|^2 + \left(\frac{2L}{\mu^2} + \frac{1}{\mu}\right) \frac{M}{2} \|d_{k+1}\|^2 + \|x_k - x^*\| \\
&\leq \frac{M}{\mu} \|x_k - x^*\|^2 + \|x_k - x^*\| + O(\|d_{k+1}\|^2).
\end{aligned}$$

By rearranging the terms, we have

$$\|d_{k+1}\| - O(\|d_{k+1}\|^2) \leq \frac{M}{\mu} \|x_k - x^*\|^2 + \|x_k - x^*\|. \quad (36)$$

From the assumption x_k converges to x^* , it holds that $d_{k+1} \rightarrow 0$, when k is sufficiently large. Thus, inequality (36) implies $\|d_{k+1}\| \leq \|x_k - x^*\|$, i.e. $\|d_{k+1}\| = O(\|x_k - x^*\|)$, which in return shows that $\|x_{k+1} - x^*\| \leq O(\|x_k - x^*\|^2)$. \square

3.4 Discussion on Assumption 2

In fact, the inequality (18) in Assumption 2 plays a crucial role in our convergence analysis. To ensure (18), a popular strategy is to apply the Lanczos method; see [8, 15, 12]. Although we can not rigorously establish the validness of Assumption 2 using merely g_k and d_k , we manage to find out that it is required only when $\lambda_k \leq \sqrt{\epsilon}$ according to Lemma 6 and the last part of the proof for Theorem 3. When it does not hold, we use a Krylov subspace method to perform one *corrector step*. For example, when $\lambda_k \leq \sqrt{\epsilon}$, this procedure iteratively includes new Krylov directions to generate a larger subspace while resolving the subproblem (5):

$$d_{k+1}^{j+1} = \arg \min m_k(d), \text{ s.t. } d \in \mathcal{L}_k^{j+1} := \text{span}\{\mathcal{L}_k^j, H_k d_{k+1}^j\}$$

until Assumption 2 is met. However, it is possible that the expanded resulted from the above method in return produces a larger $\lambda_{k+1} > \sqrt{\epsilon}$, in which case we terminate the Krylov method and proceed the main iterates. Therefore, we apply the *corrector step* periodically whenever $\lambda_k \leq \sqrt{\epsilon}$. Fortunately, for every iteration with $\lambda_k \geq \sqrt{\epsilon}$, the objective function has a amount of decrease $\frac{2}{3M^2} \epsilon^{3/2}$ (by Lemma 5). Thus the number of corrector steps is very limited when x_k is close to convergence. Finally, we terminate the algorithm as soon as $\lambda_k \leq \sqrt{\epsilon}$ and (18) hold simultaneously.

4 Applications

In this section, we provide detailed experiments of DRSOM on nonconvex optimization problems. The computational results can be divided into two parts accordingly.

- We first run DRSOM on two nonconvex problems: the $\mathcal{L}_2 - \mathcal{L}_p$ minimization and the sensor network localization.

- The rest of the experiments focus on training neural networks.

To demonstrate the efficacy of DRSSOM in the first part of experiments, we implement the algorithm using the Julia programming language for convenient comparisons to first- and second-order methods. Thus, the experiments are performed in the Julia version on a desktop of Mac OS with a 3.2 GHz 6-Core Intel Core i7 processor. The benchmark algorithms, including the (accelerated) gradient descent method, conjugate gradient method, LBFGS, and Newton trust-region method, are all from a third-party package `Optim.jl`³, including a set of line search algorithms in `LineSearches.jl`⁴.

In the second part of experiments, we implement a version in PyTorch that enables experiments in neural network training. For this part, the DRSSOM runs on a Ubuntu desktop with Intel Xeon CPU E5-2698 v4 processor and 1 NVIDIA Tesla V100. We provide a comparison of SGD and Adam. Note the SGD and Adam optimizer used in our experiments is provided by the official implementation of PyTorch⁵.

In the experiments, we use the radius-free version of DRSSOM. Let us briefly describe a strategy to update μ_k in (6). Since the ‘‘Radius-Free’’ parameter μ_k is designed as a wild estimate to λ_k for (5), we adjust μ_k by the following rule:

Let $\mu_1 \leq \mu_2$ be the eigenvalues of H_k in the subspace, consider a simple adaptive rule to put μ_k in a desired interval $[\underline{\mu}_k, \bar{\mu}_k]$:

$$\begin{aligned} \gamma_{k+1} &= \begin{cases} \beta_2 \gamma_k, & \rho_k \leq \zeta_1 \\ \max\{\underline{\gamma}, \min\{\sqrt{\gamma_k}, \beta_1 \gamma_k\}\}, & \rho_k > \zeta_2 \end{cases} \\ \underline{\mu}_k &= \max\{0, -\mu_1\} \\ \bar{\mu}_k &= \max\{\underline{\mu}_k, \mu_2\} + \mu_M \\ \mu_k &= \gamma_k \cdot \bar{\mu}_k + \max\{1 - \gamma_k, 0\} \cdot \underline{\mu}_k \end{aligned} \tag{37}$$

where $\gamma_k > 0$, μ_M is a big number to bound μ_k from above, and $\underline{\gamma}$ is the minimum level for γ_k and that $\beta_1 < 1 < \beta_2$. In the computations, we increase γ_k if the model reduction is not accurate according to ρ_k .

In the above procedure (37), we adjust μ_k with γ_k , which is expected to be less affected by the eigenvalues. If γ_k approaches to 0, then μ_k is close to $\underline{\mu}_k$ which implies \tilde{H}_k is almost positive semi-definite. Otherwise, γ_k induces a large μ_k so as to give a small trust-region radius.

4.1 $\mathcal{L}_2 - \mathcal{L}_p$ Minimization

We test the performance of DRSSOM for nonconvex $\mathcal{L}_2 - \mathcal{L}_p$ minimization widely used in compressed sensing. Recall $\mathcal{L}_2 - \mathcal{L}_p$ minimization problem (Ge et al. [18], Chen et al. [10], Chen

³For details, see <https://github.com/JuliaNLSolvers/Optim.jl>

⁴For details, see <https://github.com/JuliaNLSolvers/LineSearches.jl>

⁵For details, see <https://pytorch.org/docs/stable/generated/torch.optim.Adam.html>

[9]):

$$\min_{x \in \mathbb{R}^m} \phi(x) = \frac{1}{2} \|Ax - b\|_2^2 + \lambda \|x\|_p^p, \quad (38)$$

where $A \in \mathbb{R}^{n \times m}$, $b \in \mathbb{R}^n$, $0 < p < 1$. To overcome nonsmoothness of $\|\cdot\|_p$, we apply the smoothing strategy mentioned in Chen [9]:

$$f(x) = \frac{1}{2} \|Ax - b\|_2^2 + \lambda \sum_{i=1}^n s(x_i, \varepsilon)^p, \quad (39)$$

where $s(x_i, \varepsilon)$ is a piece-wise approximation of $|x_i|$ and ε is a small pre-defined constant $\varepsilon > 0$:

$$s(x, \varepsilon) = \begin{cases} |x| & \text{if } |x| > \varepsilon \\ \frac{x^2}{2\varepsilon} + \frac{\varepsilon}{2} & \text{if } |x| \leq \varepsilon \end{cases} \quad (40)$$

We randomly generate datasets with different sizes n, m based on the following procedure. The elements of matrix A are generated by $A_{ij} \sim \mathcal{N}(0, 1)$ with sparsity of $r = 15\%, 25\%$. To construct the true sparse vector $v \in \mathbb{R}^m$, we let for all i :

$$v_i \sim \begin{cases} 0 & \text{with probability } p = 0.5 \\ \mathcal{N}(0, \frac{1}{n}) & \text{otherwise} \end{cases}$$

Then we let $b = Av + \delta$ where δ is the noise generated as $\delta_i \sim \mathcal{N}(0, 1)$ for all i . The parameter λ is chosen as $\frac{1}{5} \|A^T b\|_\infty$. We generate instances for (n, m) from $(300, 100)$ to $(1000, 500)$. We set $p = 0.5$ and the smoothing parameter $\varepsilon = 1e^{-1}$.

Next, we test the performance of DRSON and benchmark algorithms including two first-order representative GD and Hager-Zhang nonlinear conjugate gradient method CG, and two second-order methods LBFGS and the Newton trust-region method (Newton-TR). The GD is enhanced with the Hager-Zhang line-search algorithm (see [47]) for global convergence. We report the iteration number to reach a first-order stationary point at a precision of $1e^{-5}$, precisely,

$$|\nabla f(x_k)| \leq \epsilon := 1e^{-5}.$$

The iterations and running time needed for a set of methods are reported in the Table 1. These results show that the DRSON is fairly close to LBFGS and CG and also the full-dimensional second-order methods, especially the Newton trust-region method; it is far better than GD in most test instances.

4.2 Sensor Network Localization

We next test another nonconvex optimization problem, namely, the Sensor Network Localization (SNL). The SNL problem is to find coordinates of ad hoc wireless sensors given pairwise distances in the network. Fruitful research has been found for this problem, among which the approach based on Semidefinite Programming Relaxation (SDR) has witnessed great success; see, for

| n | m | r | DRSOM | | GD | | CG | | LBFSGS | | Newton-TR | |
|------|-----|---------|-------|---------|-------|---------|-----|---------|--------|---------|-----------|---------|
| | | | k | time | k | time | k | time | k | time | k | time |
| 300 | 100 | 1.5e-01 | 101 | 9.1e-02 | 810 | 3.8e-01 | 85 | 2.6e-02 | 122 | 1.7e-01 | 10 | 4.3e-02 |
| 300 | 200 | 1.5e-01 | 176 | 1.3e-01 | 3300 | 4.3e-01 | 175 | 4.3e-02 | 207 | 2.6e-02 | 16 | 1.7e-01 |
| 300 | 500 | 1.5e-01 | 304 | 1.8e-01 | 3954 | 1.2e+00 | 262 | 1.3e-01 | 280 | 6.8e-02 | 29 | 1.8e+00 |
| 500 | 100 | 1.5e-01 | 117 | 2.3e-02 | 818 | 7.3e-02 | 71 | 1.0e-02 | 84 | 6.0e-03 | 10 | 2.0e-02 |
| 500 | 200 | 1.5e-01 | 199 | 6.6e-02 | 2682 | 5.0e-01 | 234 | 6.2e-02 | 224 | 4.4e-02 | 98 | 9.7e-01 |
| 500 | 500 | 1.5e-01 | 306 | 2.7e-01 | 5301 | 1.9e+00 | 255 | 1.6e-01 | 208 | 8.1e-02 | 27 | 1.8e+00 |
| 1000 | 100 | 1.5e-01 | 134 | 4.1e-02 | 985 | 1.6e-01 | 115 | 2.5e-02 | 144 | 1.9e-02 | 54 | 2.0e-01 |
| 1000 | 200 | 1.5e-01 | 314 | 1.4e-01 | 2327 | 5.9e-01 | 283 | 9.9e-02 | 256 | 5.2e-02 | 50 | 4.8e-01 |
| 1000 | 500 | 1.5e-01 | 315 | 3.2e-01 | 5047 | 2.8e+00 | 446 | 3.9e-01 | 308 | 1.8e-01 | 57 | 3.2e+00 |
| 300 | 100 | 2.5e-01 | 211 | 4.0e-02 | 2048 | 1.8e-01 | 227 | 2.8e-02 | 228 | 1.5e-02 | 70 | 1.6e-01 |
| 300 | 200 | 2.5e-01 | 263 | 1.3e-01 | 5724 | 6.8e-01 | 225 | 4.0e-02 | 231 | 2.8e-02 | 69 | 7.2e-01 |
| 300 | 500 | 2.5e-01 | 401 | 2.3e-01 | 10000 | 2.7e+00 | 296 | 2.4e-01 | 372 | 1.0e-01 | 125 | 6.9e+00 |
| 500 | 100 | 2.5e-01 | 161 | 3.7e-02 | 1784 | 1.4e-01 | 170 | 2.3e-02 | 190 | 1.4e-02 | 55 | 1.8e-01 |
| 500 | 200 | 2.5e-01 | 297 | 1.0e-01 | 5095 | 7.8e-01 | 212 | 5.5e-02 | 228 | 1.0e-01 | 90 | 9.1e-01 |
| 500 | 500 | 2.5e-01 | 405 | 2.9e-01 | 9897 | 3.6e+00 | 356 | 2.4e-01 | 361 | 1.2e-01 | 209 | 1.3e+01 |
| 1000 | 100 | 2.5e-01 | 173 | 1.1e-01 | 3799 | 5.0e-01 | 180 | 6.5e-02 | 176 | 1.7e-02 | 51 | 1.3e-01 |
| 1000 | 200 | 2.5e-01 | 286 | 2.1e-01 | 4954 | 1.1e+00 | 245 | 1.2e-01 | 285 | 6.4e-02 | 120 | 1.3e+00 |
| 1000 | 500 | 2.5e-01 | 343 | 3.6e-01 | 7889 | 4.3e+00 | 261 | 2.8e-01 | 316 | 1.6e-01 | 118 | 8.8e+00 |

Table 1: Performance of DRSOM on (38) compared to other algorithms: iterations needed for precision $\epsilon = 1e^{-5}$

example, Biswas and Ye [3], Wang et al. [35], and many others. We here adopt the notations in [35].

Let n sensors be points in \mathbb{R}^d , besides, assume another set of m *known* points (usually referred to as anchors) whose exact positions are a_1, \dots, a_m . Let d_{ij} be the distance between sensor i and j , and \bar{d}_{ik} be the distance from the sensor i to anchor point k . We can then define the set of distances as edges in the network:

$$N_x = \{(i, j) : \|x_i - x_j\| = d_{ij} \leq r_d\}, N_a = \{(i, k) : \|x_i - a_k\| = \bar{d}_{ik} \leq r_d\}, \quad (41)$$

where r_d is a fixed parameter known as the *radio range*. Using these given set of distances, the SNL problem is to find other the exact positions of left $n - m$ sensors. In the following, we specifically consider $d = 2$ such that the solutions to this problem can be visualized. Formally, the SNL problem considers the following quadratic constrained quadratic programming (QCQP) feasibility problem,

$$\|x_i - x_j\|^2 = d_{ij}^2, \forall (i, j) \in N_x \quad (42a)$$

$$\|x_i - a_k\|^2 = \bar{d}_{ik}^2, \forall (i, k) \in N_a \quad (42b)$$

which can be solved by a nonlinear least-square (NLS) problem:

$$\min_X \sum_{(i < j, j) \in N_x} (\|x_i - x_j\|^2 - d_{ij}^2)^2 + \sum_{(k, j) \in N_a} (\|a_k - x_j\|^2 - \bar{d}_{kj}^2)^2, \quad (43)$$

which is clearly nonconvex. Instead of directly solving (43), one classical framework is to apply the *two-stage* strategy proposed in Biswas and Ye [3]. In the first stage, we use semidefinite

programming to solve a lifted convex relaxation to (43):

$$\begin{aligned}
& \min 0 \bullet Z \\
& \text{s.t. } Z_{[1:2,1:2]} = I, \\
& (0; e_i - e_j) (0; e_i - e_j)^T \bullet Z = d_{ij}^2 \quad \forall (i, j) \in N_x, \\
& (-a_k; e_i) (-a_k; e_i)^T \bullet Z = d_{ik}^2 \quad \forall (i, k) \in N_a \\
& Z \succeq 0,
\end{aligned} \tag{44}$$

where we let I be the identity matrix of dimension 2, e_i be a n -vector of zeros except for a one at i -th entry. Z is the lifted positive semidefinite matrix, such that

$$Z = \begin{bmatrix} I & X \\ X^T & Y \end{bmatrix}, \tag{45}$$

which is equivalent to state $Y \succeq X^T X$. If the solution of SDR satisfies $\text{rank } Y = 2$, then SDR solves the original problem; otherwise, (Y, X) is used to initialize the NLS problem for further refinement in the second stage. In the original work of [3], local solutions of (43) are pursued by the gradient descent method (GD). To set a comparison, we use DRSOM and CG in place for GD.

4.2.1 A specific example where DRSOM produces better solutions

We here provide a randomly generated example with 80 points, 5 of which are anchors. We set the radio range to 0.5 and the random distance noise $n_f = 0.05$. We terminate at an iterate x_k if $\|g(x_k)\| \leq 1e^{-6}$.

Our computational results of this example basically illustrate that if we initialize the NLS problem (43) for SNL by the SDR (44), then DRSOM and GD are comparable. However, if we do not have the SDR solution at hand, the DRSOM may usually provide better solutions than GD, which shows the benefits of exploring second-order information in a very limited subspace.

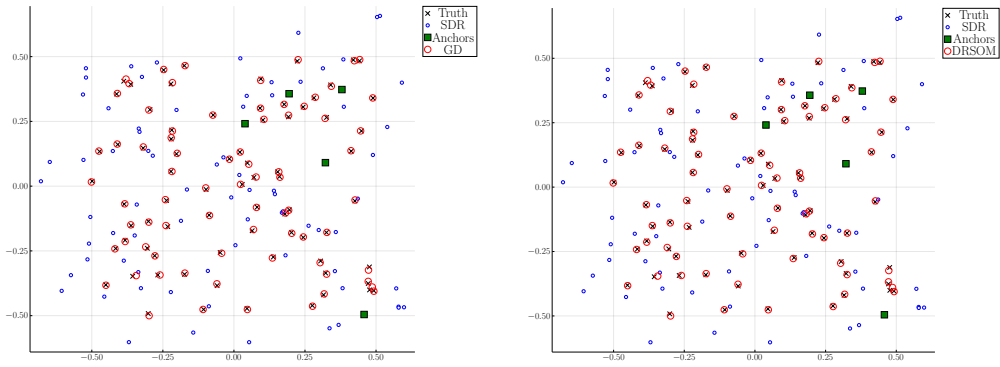
Figure 1 depicts the realization results of GD and DRSOM initialized by SDP relaxation. In this case, both algorithms are able to guarantee convergence to the ground truth.

As a comparison, Figure 2 depicts the case without solving SDR first. We use the same parameter settings as for the previous case. The GD and DRSOM initializes with $X_i := 0, i = 1, \dots, n$ and both solves to $\|g(x_k)\| \leq 1e^{-6}$. In this particular case, the GD fails to recover true positions; however, the DRSOM can provide accurate solutions even without the SDR initialization.

In this example, we rigorously provide a case where the DRSOM may result in a better solution (in this case, the global one) than the first-order methods despite that we only have optimal subspace guarantees in theory.

4.2.2 Solving large SNL instances

In this part, we compare GD, CG, and DRSOM on large SNL instances up to 10,000 sensors. Similar to the previous tests, CG and GD are facilitated with Hager-Zhang line search algorithm.



(a) The graphic result of GD initialized by an SDR solution (b) The graphic result of DRSOM initialized by an SDR solution

Figure 1: Comparison of localization by GD and DRSOM with SDR initialization. The **rectangles** and **crosses** represent the anchors and true locations, respectively. The blue **circles** are solutions by SDR, and the red **circles** are final solutions of GD/DRSOM.

We terminate an algorithm if $\|g_k\| \leq 1e^{-5}$ or the running time exceeds 3,000 seconds.

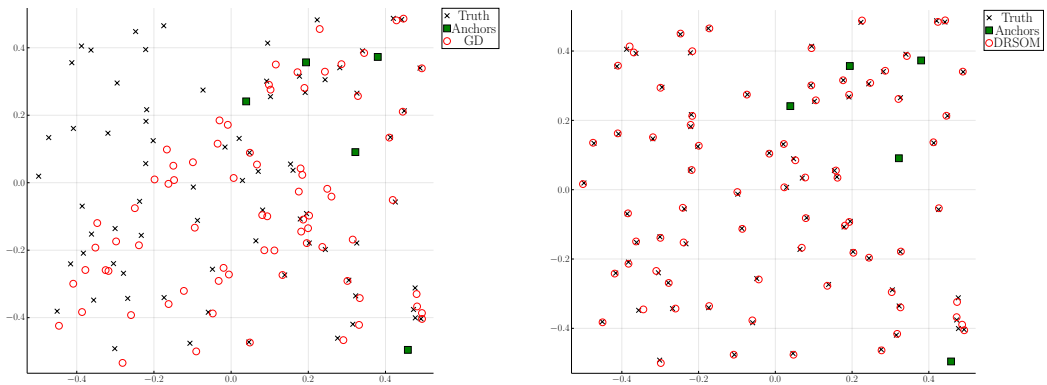
Our results are presented in [Table 2](#) and [Table 3](#). The GD fails to converge if the number of sensors exceeds 3,000. DRSOM has a clear edge over CG in most case; furthermore, it solves the problem with 10,000 sensors in about 2,200 seconds.

| n | m | $ E $ | k | | | $\ g\ $ | | |
|-------|------|---------|---------|---------|---------|---------|---------|---------|
| | | | CG | DRSOM | GD | CG | DRSOM | GD |
| 500 | 50 | 2.2e+04 | 1.2e+02 | 9.0e+01 | 3.2e+02 | 7.0e-06 | 6.8e-06 | 9.4e-06 |
| 1000 | 80 | 4.6e+04 | 2.3e+02 | 2.1e+02 | 1.4e+03 | 7.0e-06 | 8.6e-06 | 9.9e-06 |
| 2000 | 120 | 9.4e+04 | 4.5e+02 | 4.2e+02 | 4.4e+03 | 8.4e-06 | 8.4e-06 | 9.9e-06 |
| 3000 | 150 | 1.4e+05 | 7.4e+02 | 4.2e+02 | 7.5e+03 | 8.9e-06 | 8.4e-06 | 1.6e-03 |
| 4000 | 400 | 1.8e+05 | 1.2e+03 | 7.8e+02 | - | 7.9e-06 | 9.8e-06 | - |
| 6000 | 600 | 2.7e+05 | 1.2e+03 | 1.1e+03 | - | 9.2e-06 | 8.8e-06 | - |
| 10000 | 1000 | 4.5e+05 | 1.0e+03 | 1.5e+03 | - | 2.3e-03 | 9.0e-06 | - |

Table 2: Iteration number and gradient error of CG, DRSOM, and GD on SNL instances. n and m denotes the number of sensors and anchors. $|E|$ denotes the number of used edges (QCQP constraints). “-” means the algorithm exceeds 3,000s.

| n | m | $ E $ | t | | |
|-------|------|---------|---------|---------|---------|
| | | | CG | DRSOM | GD |
| 500 | 50 | 2.2e+04 | 1.7e+01 | 1.1e+01 | 2.3e+01 |
| 1000 | 80 | 4.6e+04 | 7.3e+01 | 3.9e+01 | 1.8e+02 |
| 2000 | 120 | 9.4e+04 | 2.5e+02 | 1.4e+02 | 1.1e+03 |
| 3000 | 150 | 1.4e+05 | 6.5e+02 | 1.4e+02 | - |
| 4000 | 400 | 1.8e+05 | 1.3e+03 | 5.0e+02 | - |
| 6000 | 600 | 2.7e+05 | 2.0e+03 | 1.1e+03 | - |
| 10000 | 1000 | 4.5e+05 | - | 2.2e+03 | - |

Table 3: Running time of CG, DRSOM, and GD on SNL instances of different problem size, $|E|$ denotes the number of QCQP constraints. “-” means the algorithm exceeds 3,000s.



(a) The graphic result of GD without an SDR solution (b) The graphic result of DRSOM without an SDR solution

Figure 2: Comparison of localization by GD and DRSOM without SDR initialization. The meaning of each symbol is the same as Figure 1.

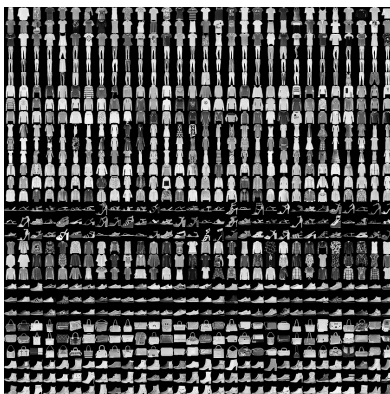


Figure 3: A sample collection of the Fashion-MNIST ⁶

4.3 Neural Networks

In this subsection, we implement a vanilla Mini-Batch DRSOM to train neural networks. Our implementation is straightforward: for each mini-batch, we calculate the required gradients and compute extra function evaluations. Then we use the interpolation method to find estimates of Q_k . The main algorithm proceeds just like the “full-batch” version. Finally, we test two Mini-Batch DRSOM variants using the gradient only (DRSOM-g) and gradient and momentum (DRSOM-g+d) and compare the performance with the SGD and Adam optimizer.

4.3.1 Fashion-MNIST

We train a Neural Network model for classification on Fashion-MNIST (see Figure 3), consisting of a training set of 60,000 examples and a test set of 10,000 examples [37]. The dataset is constructed from images with one of 10 labels, including T-shirt/top, bag, dress and so on. In our test, we adopt a neural network model with two convolutional and two fully-connected layers⁷, which has about 16.84 million parameters. For SGD, we test on different momentum coefficients $\mu \in \{0.9, 0.95, 0.99\}$ named after SGDm- μ . Also, the Adam and SGD are set with the learning rate at $1e^{-3}$. All optimizers are tested with a batch size of 128.

From Table 4 and Figure 4, we see that in 20 epochs, the Adam, SGD (SGDm- μ), and DRSOM are both able to reach over 90% accuracy on the hold-out test set. Both DRSOM-g and DRSOM-g+d, even with a naive mini-batch strategy, are the best in terms of loss and accuracy in the training set. They also have the best test accuracy compared to the competitors. In our experiments, DRSOM is about 1.2 times slower than Adam per-epoch in this case.

⁶For details, see <https://github.com/zalandoresearch/fashion-mnist>

⁷For details, see <https://github.com/ashmeet13/FashionMNIST-CNN/blob/master/Fashion.py>

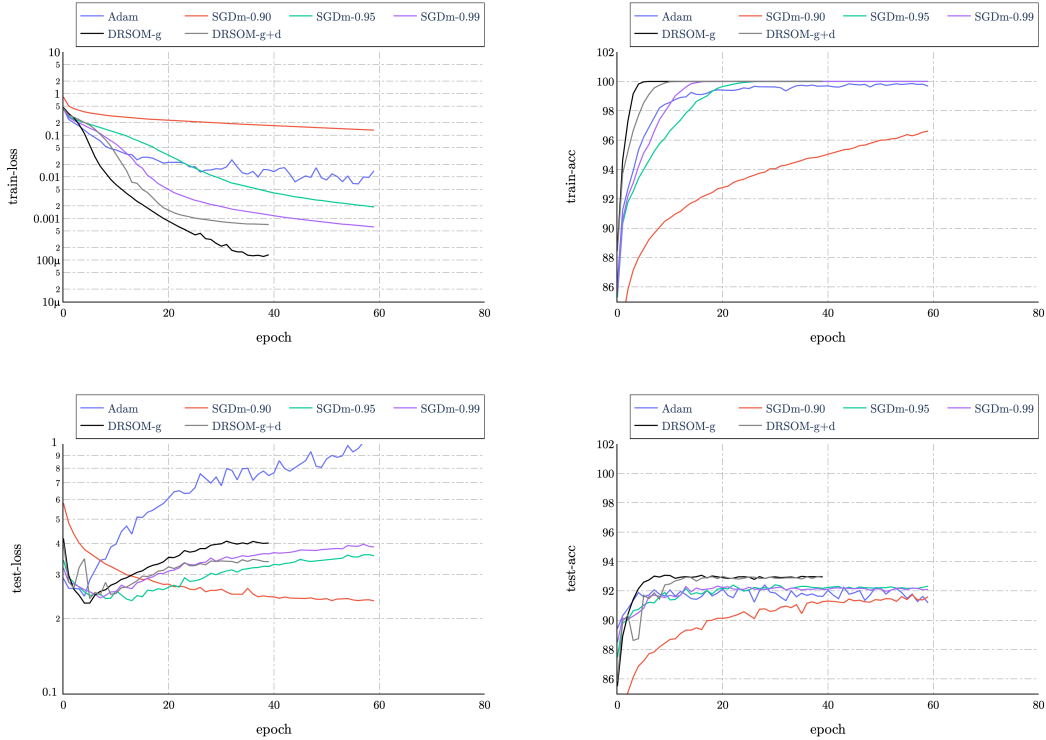


Figure 4: Training and test results of Adam, SGD, and DRSOM for a Neural network on Fashion-MNIST dataset

4.3.2 CIFAR10

To further take a look in *deep* neural networks, we also train ResNet18 and ResNet34 (He et al. [21]) for CIFAR10. We run ADAM, SGDm- μ , and variants of DRSOM for 80 epochs with a batch size of 128. For Adam, we provide a learning rate scheduler to decay the learning rate by a factor of 2 in every k epochs started at an initial rate $1e^{-3}$; we test the same variants of SGD similar to the previous section.

To enable fair comparison, for DRSOM, we increase the lower bound of $\underline{\gamma}$ by the rule, $\underline{\gamma} := \underline{\gamma} \cdot 1000$, in every 10 epochs corresponding to the update policy (37). We apply the strategy to mimic a mechanism of reducing the learning rate. We report the test results in Table 5 and Figure 5.

As the results show, DRSOM-g and DRSOM-g+d still permit sharp rates of increase in the beginning of training; with little tuning efforts, they also have competitive results to Adam and SGD in 80 epochs. However, compared to easier architectures in previous section, DRSOM-g and DRSOM-g+d do not benefit clearly in this case. This is partially due to stochastic noises and complex architectures in these models that may bring significant inexactness to the current

| Method | Training Acc. | Test Acc. |
|-----------|---------------|-----------|
| Adam | 99.68% | 91.18% |
| SGDm-0.9 | 99.61% | 91.6% |
| SGDm-0.95 | 99.99% | 92.32% |
| SGDm-0.99 | 99.99% | 92.1% |
| DRSOM-g | 99.99% | 92.97% |
| DRSOM-g+d | 99.99% | 92.92% |

Table 4: Training and Test accuracy of test methods on Fashion-MNIST

| Method | Test Acc. (ResNet18) | Test Acc. (ResNet34) |
|-----------|----------------------|----------------------|
| Adam | 92.98% | 93.29% |
| SGDm-0.9 | 89.57% | 90.27% |
| SGDm-0.95 | 91.29% | 91.28% |
| SGDm-0.99 | 92.31% | 92.69% |
| DRSOM-g | 92.27% | 93.23% |
| DRSOM-g+d | 92.14% | 92.98% |

Table 5: Test accuracy of the methods on ResNet18 and ResNet34 for CIFAR10

interpolation scheme. As we note from the training and test curves, the accuracy and loss may fluctuate heavily during the process and are less stable compared to those in the previous example. However, these preliminary results, to our belief, motivate future research and better implementation of the DRSOM.

5 Conclusion

In this paper, we introduce a Dimension-Reduced Second-order Method (DRSOM) that utilizes 2-D trust-region subproblems and requires only the gradient, momentum, and two extra Hessian-vector products (alternatively, interpolation with three function evaluations) that cost almost the same as first-order methods. We give a concise analysis of the global and local speed of convergence. Computationally, we provide fruitful examples in nonconvex optimization and deep learning. Notably, DRSOM has substantial superiority to first-order methods while keeping a low cost per iteration compared to second-order methods.

Our preliminary results motivate future developments of DRSOM. In terms of [Assumption 2](#), it is an important aspect to find more efficient approach to satisfy (18) in addition to the Krylov subspace method. For deep learning, it is possible to survey enhancements such as the Kronecker-factored curvature and subsampling techniques to speed up the iterations of DRSOM.

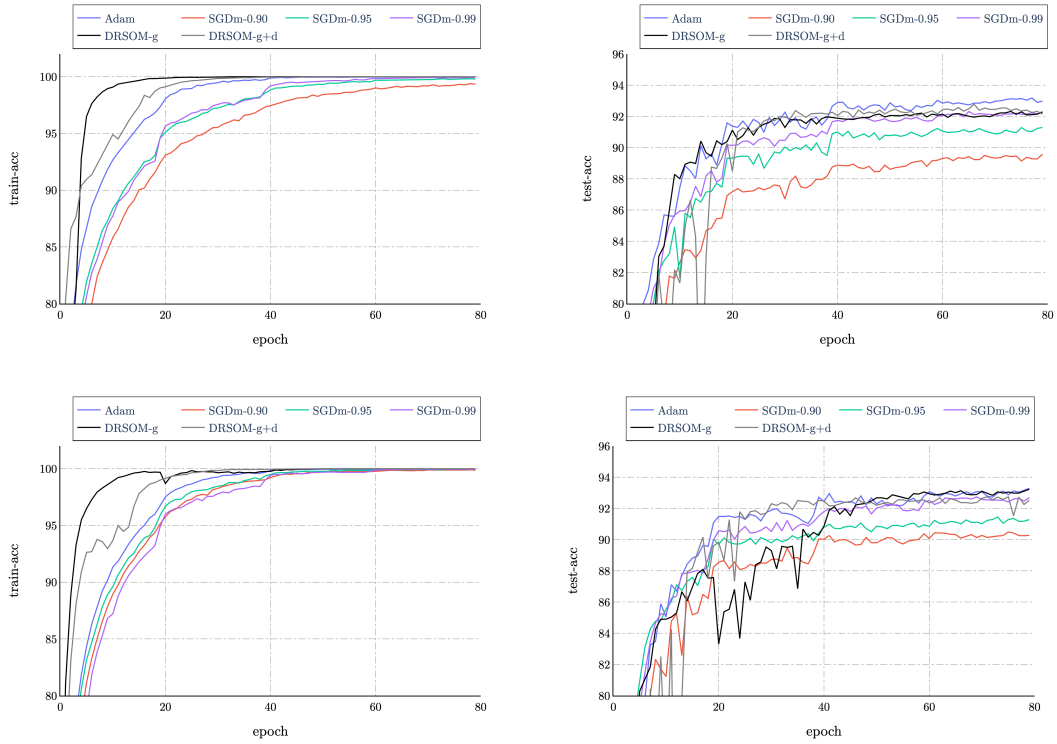


Figure 5: Training and test results of Adam and DRSOM for ResNet18 and ResNet34 on CIFAR10

Acknowledgement

The authors would like to thank Tianyi Lin for the insightful comments that significantly improve the presentation of this paper.

References

- [1] Vassilis Apidopoulos, Nicolò Ginatta, and Silvia Villa. Convergence rates for the heavy-ball continuous dynamics for non-convex optimization, under Polyak–Łojasiewicz condition. *Journal of Global Optimization*, 84(3):563–589, November 2022.
- [2] Albert S. Berahas, Raghu Bollapragada, and Jorge Nocedal. An investigation of Newton-Sketch and subsampled Newton methods. *Optimization Methods and Software*, 35(4):661–680, July 2020.
- [3] Pratik Biswas and Yinyu Ye. Semidefinite programming for ad hoc wireless sensor network localization. In *Third International Symposium on Information Processing in Sensor Networks, IPSN 2004*, pages 46–54, 2004.
- [4] Yair Carmon, Oliver Hinder, John C. Duchi, and Aaron Sidford. Convex Until Proven Guilty: Dimension-Free Acceleration of Gradient Descent on Non-Convex Functions, May 2017.
- [5] Yair Carmon, John C. Duchi, Oliver Hinder, and Aaron Sidford. Accelerated Methods for NonConvex Optimization. *SIAM Journal on Optimization*, 28(2):1751–1772, January 2018.
- [6] C. Cartis, N. I. M. Gould, and Ph. L. Toint. On the Complexity of Steepest Descent, Newton’s and Regularized Newton’s Methods for Nonconvex Unconstrained Optimization Problems. *SIAM Journal on Optimization*, 20(6):2833–2852, January 2010.
- [7] Coralia Cartis, Nicholas I. M. Gould, and Philippe L. Toint. Adaptive cubic regularisation methods for unconstrained optimization. Part II: worst-case function- and derivative-evaluation complexity. *Mathematical Programming*, 130(2):295–319, December 2011.
- [8] Coralia Cartis, Nicholas I. M. Gould, and Philippe L. Toint. Adaptive cubic regularisation methods for unconstrained optimization. Part I: motivation, convergence and numerical results. *Mathematical Programming*, 127(2):245–295, April 2011.
- [9] Xiaojun Chen. Smoothing methods for nonsmooth, nonconvex minimization. *Mathematical Programming*, 134(1):71–99, August 2012.
- [10] Xiaojun Chen, Dongdong Ge, Zizhuo Wang, and Yinyu Ye. Complexity of unconstrained $L_2 - L_p$ minimization. *Mathematical Programming*, 143(1-2):371–383, February 2014.
- [11] A. R. Conn, Katya Scheinberg, and Luis N. Vicente. *Introduction to derivative-free optimization*. Number 8 in MPS-SIAM series on optimization. Society for Industrial and Applied Mathematics/Mathematical Programming Society, Philadelphia, 2009.
- [12] Andrew R. Conn, Nicholas IM Gould, and Philippe L. Toint. *Trust region methods*. SIAM, 2000.
- [13] Andrew R. Conn, Katya Scheinberg, and Luís N. Vicente. Geometry of interpolation sets in derivative free optimization. *Mathematical programming*, 111(1):141–172, 2008.

- [14] Andrew R. Conn, Katya Scheinberg, and Luís N. Vicente. Global convergence of general derivative-free trust-region algorithms to first-and second-order critical points. *SIAM Journal on Optimization*, 20(1):387–415, 2009.
- [15] Frank E. Curtis, Daniel P. Robinson, and Mohammadreza Samadi. A trust region algorithm with a worst-case iteration complexity of $\mathcal{O}(\epsilon^{-3/2})$ for nonconvex optimization. *Mathematical Programming*, 162(1):1–32, March 2017.
- [16] Frank E. Curtis, Michael J. O’Neill, and Daniel P. Robinson. Worst-Case Complexity of an SQP Method for Nonlinear Equality Constrained Stochastic Optimization, January 2022.
- [17] John E. Dennis and Jorge J. Moré. Quasi-Newton methods, motivation and theory. *SIAM review*, 19(1):46–89, 1977.
- [18] Dongdong Ge, Xiaoye Jiang, and Yinyu Ye. A note on the complexity of Lp minimization. *Mathematical Programming*, 129(2):285–299, 2011.
- [19] Euhanna Ghadimi, Hamid Reza Feyzmahdavian, and Mikael Johansson. Global convergence of the Heavy-ball method for convex optimization. In *2015 European Control Conference (ECC)*, pages 310–315, Linz, Austria, July 2015.
- [20] William W. Hager and Hongchao Zhang. Algorithm 851: CG_descent, a conjugate gradient method with guaranteed descent. *ACM Transactions on Mathematical Software (TOMS)*, 32(1):113–137, 2006.
- [21] Kaiming He, Xiangyu Zhang, Shaoqing Ren, and Jian Sun. Deep residual learning for image recognition. In *Proceedings of the IEEE conference on computer vision and pattern recognition*, pages 770–778, 2016.
- [22] Diederik P. Kingma and Jimmy Ba. Adam: A method for stochastic optimization. *arXiv preprint arXiv:1412.6980*, 2014.
- [23] Jonathan Lacotte, Yifei Wang, and Mert Pilanci. Adaptive newton sketch: Linear-time optimization with quadratic convergence and effective hessian dimensionality. In *International Conference on Machine Learning*, pages 5926–5936. 2021.
- [24] Xin Liu, Zaiwen Wen, and Yaxiang Yuan. Subspace Methods for Nonlinear Optimization, 2021.
- [25] David G. Luenberger and Yinyu Ye. *Linear and Nonlinear Programming*, volume 228 of *International Series in Operations Research & Management Science*. Springer International Publishing, Cham, 2021.
- [26] Yurii Nesterov. *Lectures on convex optimization*, volume 137. Springer, 2018.
- [27] Yurii Nesterov and B.T. Polyak. Cubic regularization of Newton method and its global performance. *Mathematical Programming*, 108(1):177–205, August 2006.

- [28] Jorge Nocedal and Stephen Wright. *Numerical optimization*. Springer Science & Business Media, 2006.
- [29] Peter Ochs, Yunjin Chen, Thomas Brox, and Thomas Pock. ipiano: Inertial proximal algorithm for nonconvex optimization. *SIAM Journal on Imaging Sciences*, 7(2):1388–1419, 2014.
- [30] Mert Pilanci and Martin J. Wainwright. Newton sketch: A near linear-time optimization algorithm with linear-quadratic convergence. *SIAM Journal on Optimization*, 27(1):205–245, 2017.
- [31] B. T. Polyak. Some methods of speeding up the convergence of iteration methods. *USSR Computational Mathematics and Mathematical Physics*, 4(5):1–17, January 1964.
- [32] Tao Sun, Dongsheng Li, Zhe Quan, Hao Jiang, Shengguo Li, and Yong Dou. Heavy-ball algorithms always escape saddle points. *arXiv preprint arXiv:1907.09697*, 2019.
- [33] Tao Sun, Penghang Yin, Dongsheng Li, Chun Huang, Lei Guan, and Hao Jiang. Non-Ergodic Convergence Analysis of Heavy-Ball Algorithms. *Proceedings of the AAAI Conference on Artificial Intelligence*, 33(01):5033–5040, July 2019.
- [34] Zhou-Hong Wang and Ya-Xiang Yuan. A subspace implementation of quasi-Newton trust region methods for unconstrained optimization. *Numerische Mathematik*, 104(2):241–269, August 2006.
- [35] Zizhuo Wang, Song Zheng, Yinyu Ye, and Stephen Boyd. Further relaxations of the semidefinite programming approach to sensor network localization. *SIAM Journal on Optimization*, 19(2):655–673, 2008.
- [36] David P. Woodruff. Sketching as a tool for numerical linear algebra. *Foundations and Trends® in Theoretical Computer Science*, 10(1–2):1–157, 2014.
- [37] Han Xiao, Kashif Rasul, and Roland Vollgraf. Fashion-MNIST: a Novel Image Dataset for Benchmarking Machine Learning Algorithms, August 2017.
- [38] Peng Xu, Fred Roosta, and Michael W. Mahoney. Newton-type methods for non-convex optimization under inexact Hessian information. *Mathematical Programming*, 184(1-2):35–70, November 2020.
- [39] Minghan Yang, Dong Xu, Qiwen Cui, Zaiwen Wen, and Pengxiang Xu. NG+ : A Multi-Step Matrix-Product Natural Gradient Method for Deep Learning, June 2021.
- [40] Minghan Yang, Dong Xu, Zaiwen Wen, Mengyun Chen, and Pengxiang Xu. Sketch-Based Empirical Natural Gradient Methods for Deep Learning. *Journal of Scientific Computing*, 92(3):94, September 2022.
- [41] Yinyu Ye. A New Complexity Result on Minimization of a Quadratic Function with a

- Sphere Constraint. In *Recent Advances in Global Optimization*, volume 176, pages 19–31. Princeton University Press, 1991.
- [42] Yinyu Ye. *Second Order Optimization Algorithms I*, 2005.
- [43] Y.-X. Yuan and J. Stoer. A subspace study on conjugate gradient algorithms. *ZAMM-Journal of Applied Mathematics and Mechanics/Zeitschrift für Angewandte Mathematik und Mechanik*, 75(1):69–77, 1995.
- [44] Ya-xiang Yuan. A review on subspace methods for nonlinear optimization. In *Proceedings of the International Congress of Mathematics*, pages 807–827, 2014.
- [45] Ya-xiang Yuan. Recent advances in trust region algorithms. *Mathematical Programming*, 151(1):249–281, 2015.
- [46] SK Zavriev and FV Kostyuk. Heavy-ball method in nonconvex optimization problems. *Computational Mathematics and Modeling*, 4(4):336–341, 1993.
- [47] Hongchao Zhang and William W. Hager. A nonmonotone line search technique and its application to unconstrained optimization. *SIAM journal on Optimization*, 14(4):1043–1056, 2004.